



Microanalysis of TiN phases formed in inclusions of electrogas weld metal

Kangmyung Seo¹ · Yongjoon Kang¹ · Hee Jin Kim² · Joong Geun Yoon²

Received: 18 December 2022 / Accepted: 22 March 2023 / Published online: 6 April 2023
© The Author(s) 2023

Abstract

This study has been conducted to confirm the formation of TiN phase in the electrogas (EG) weld metal and, if it formed, to identify the nucleation potency of TiN for acicular ferrite. To facilitate this, a high-nitrogen EG weld metal deposited using a very high heat input was chosen. Inclusion analyses were mostly carried out in a scanning electron microscope (SEM) and analytical transmission electron microscope (TEM) equipped with energy dispersive analyzer (EDS) and electron energy loss spectroscopy (EELS). It was confirmed that the inclusions were nearly fully covered by TiO layer alloyed with a small amount of nitrogen, this TiO layer being partly coated with TiN phases having two different types of morphology: layer-type or patch-type. The layer-type was identified to be nearly pure TiN, being formed with a thickness of 10 nm on the outer surface of thick TiO layer. The patch-type appeared to be formed on the TiN/TiO layer and was characterized by its fine lamellar mixture of TiN and (Al,Mn)-oxide. As all these phases formed on the inclusion surface, they were suspected to influence the nucleation potency of inclusions but the relative potency of these phases to TiO layer was not clearly understood.

Keywords EG welding · C-Mn steel · Acicular ferrite · Inclusion

1 Introduction

Basically, the non-metallic inclusions present in the steel weld metals are the products of deoxidation and desulphurization reactions taking place within the weld pool. These inclusions are now well established to play an important role in the microstructural development of ferritic weld metals as they can act as the nucleation sites for the acicular ferrite (AF) to form a fine weld microstructure and in turn, improve weld metal toughness [1]. However, certain types of inclusion appeared not to act as nucleation sites of AF resulting in a weld microstructure dominant with ferrite with second phase (FS). These findings have led to a lot of investigation

to identify the inclusion characteristics responsible for the ferrite nucleation, a special attention being paid to titanium-containing welds as the titanium addition showed a dramatic change of weld microstructure from FS-dominant to AF-dominant [2–7]. Following the efforts made for the titanium-containing welds, various inclusion phases such as TiO [8–10], MnTi₂O₄ [11–15], Ti₂O₃ [16, 17], and TiN [18, 19] could be identified as the ones contributing to AF nucleation. Among the phases mentioned, however, TiN appeared to have conflicting claims for the nucleation potency.

In the case of steel material, many researchers [20–24] have performed extensive studies on the role of TiN and reported that TiN particles or phases played an active role for nucleating intragranular ferrite (IGF), which is a terminology of AF often used in the literature of steel metallurgy. However, a group of other researchers [25–28] reported that single TiN particles were not effective to enable IGF nucleation or that they were less potent than titanium oxides. From the literature reviewed above, it is apparent that the nucleation potency of TiN has not been agreed for the steel material and for some reasons, can vary greatly depending on the condition of steels studied.

On the other hand, in the case of weld metals, not many references could be found. In 1970s, Ito et al. [29] firstly

Recommended for publication by Commission IX - Behaviour of Metals Subjected to Welding

✉ Hee Jin Kim
kimheejin0827@gmail.com

¹ Korea Institute of Materials Science, 797, Changwon-Daero, Seongsan-Gu, Changwon-Si, Gyeongsangnam-Do 51508, Republic of Korea

² R&D Center, KISWEL, 704 Gongdan-Ro, Seongsan-Gu, Changwon-Si, Gyeongnam 51544, Republic of Korea

mentioned the possible role of TiN for AF formation. They performed the internal friction tests and found the absence of free nitrogen in a titanium-containing weld and thus suspected that all nitrogen contained have combined with titanium on the cooling stage to form TiN precipitates. However, they did not provide the direct evidence of TiN precipitates being formed. Even then, many researchers failed to obtain the experimental evidence of TiN formation although they have studied the high-nitrogen weld metals [18, 30, 31]. This failure was explained to be most likely due to TiN phase being small in size compared to the spatial resolution limit of the analytical microscopes employed [11]. Considering that the precipitates grow by the diffusional process, the prolonged cooling time associating with the increase in welding heat input would help TiN particles get bigger on the cooling stage of weld thermal cycles. In fact, present authors [32] could observe the TiN phase formed on the inclusions of electro-gas (EG) weld metal made with a heat input as high as 20 kJ/mm and its formation was explained in terms of the high heat input employed in EG welding process.

EG welding is a vertical-up and single-pass welding process that enables to achieve a full-thickness using one or two wires depending the plate thickness. In this process, the groove openings are covered by two different materials: the back-opening by ceramic backing materials and the front-opening by water-cooled copper shoe. As the groove fills with the molten filler wires, the copper shoe moves upward along with the welding gun. As it is a full-thickness welding process, its heat input increases linearly with the plate thickness from ~20 kJ/mm for 25-mm thick plate to ~50 kJ/mm for 70-mm thick plate. These heat inputs are so high that no other processes like SMAW or GMAW can reach. Accordingly, the cooling rate from 800 to 500 °C is several hundreds of seconds in the EG welds, approximately 10 times longer than that of SMAW or AW. Following this, it was reasonably believed that the precipitation reaction of TiN phase could be enhanced by increasing the heat input of EG welds and also by increasing the nitrogen content [33].

Therefore, the purpose of the present investigation is to establish a better understanding of the morphological characteristics of TiN phase formed in the ferritic weld metal by employing a high-nitrogen EG weld deposited with a much higher heat input than that of the previous weld [32].

2 Experimental procedures

Of the EG welds investigated in the previous study [33], one designated “tandem EG(73t)” was selected for this study because its heat input of 47 kJ/mm was two times higher than that of “one-pole EG(25t)” previously studied [32]. The chemical composition quoted from the previous report is given in Table 1. As noticed in Table 1, the nitrogen content of the present weld is 116 ppm, being much higher than that of EG(25t) weld, 17 ppm. In addition to the high heat input applied, such a high level of nitrogen content was suspected to facilitate the TiN formation during the process of inclusion formation in the welds.

As noticed in its designation, this weld was fabricated by the two-pole (tandem) EG process with 73-mm thick base plates. In this vertical-up EG welding process, two flux-cored wires of 1.6 mm in diameter are generally employed and fed into a cavity formed by the groove faces of the plates to be welded. The total length of the welds was 1 m. For the present EG weld, the cooling rate from 800 to 500 °C was estimated to be 400 s using the master curves given in Reference [35].

Transverse sections were taken from the welded plate and optically examined using standard metallographic technique including grinding, polishing, and etching with 2% Nital solution. Quantitative microstructural analysis was performed using the point counting method.

Typical inclusion characteristics were first examined by field-emission scanning electron microscopy (FE-SEM, model JEOL JSM-7100F) using a metallographic specimen taken from the weld center. The chemical heterogeneity of the inclusions was analyzed by energy-dispersive X-ray spectroscopy (EDS) equipped with SEM. For the details of the inclusion constituent phases, transmission electron microscope (TEM) study was performed using thin foil samples prepared by the focused ion beam (FIB) method. The foils were examined by analytical transmission electron microscope (ATEM, model JEOL JEM-2100F) at an operating voltage of 200 kV. Of particular interest was the nature of the inclusion/matrix interface where the TiN was highly expected to be present. In addition to the orientation relationships by selected area diffraction (SAD) examination, chemical features of phases were analyzed by EDS for the major alloying elements and electron energy loss spectroscopy (EELS) for the light elements like oxygen and nitrogen in this study.

Table 1 Chemical composition of EG weld metals (wt%)

ID	C	Si	Mn	P	S	Ni	Cr	Mo	Al	Ti	B	O	N
EG (73t)	0.05	0.19	1.66	0.009	0.009	1.49	0.03	0.14	0.008	0.032	0.0043	0.0383	0.0116
EG (25t)	0.09	0.16	1.33	0.010	0.005	1.17	0.02	0.10	0.011	0.035	0.0039	0.0394	0.0017

3 Result and discussion

3.1 Macro and microstructure

The macro- and microstructures of the present weld are shown in Figs. 1a and b, respectively. As shown in the optical micrograph, the weld microstructure consists of two major constituents: grain boundary ferrite (GBF) and intragranular ferrite (IGF), IGF being a mixture of AF and polygonal ferrite (PF). Little formation of FS was also noted and this feature was mentioned to be general in the EG weld metals [34].

After the general observation given in Fig. 1b, the same specimen was used for the quantitative microstructural analysis. With the point counting method, this microstructure was able to be classified into 19% of GBF and 81% of IGF. Figure 2 shows a typical SEM microstructure taken at the region of IGF microstructure, depicting many AF plates emanating from the inclusions. It is worth mentioning that in the present weld, large inclusions over 3 μm in size were not difficult to find by virtue of its high heat input applied.

3.2 Inclusion analysis by SEM/EDS

To figure out the overall picture of constituent phases formed in inclusions, SEM/EDS analyses were first performed on the cross-sections of large inclusions, the sizes of which were over 3 μm . The SEM image in Fig. 3 represents a typical structure of inclusion in which several particles are engulfed by the matrix phase of inclusion. The EDS spot analysis performed for many inclusions showed that the matrix phase was an oxide rich in aluminum, manganese, and silicon, i.e., (Al,Mn)-silicate, while the granular particles embedded in the matrix were either titanium oxide or aluminum oxide, as shown in Fig. 3. In addition, islands of manganese sulfide (MnS) were often found in the peripheral region of inclusions. Most importantly, as evident in the titanium and nitrogen images

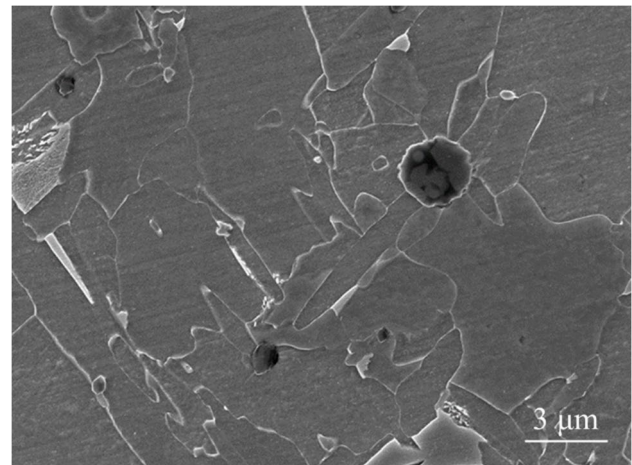
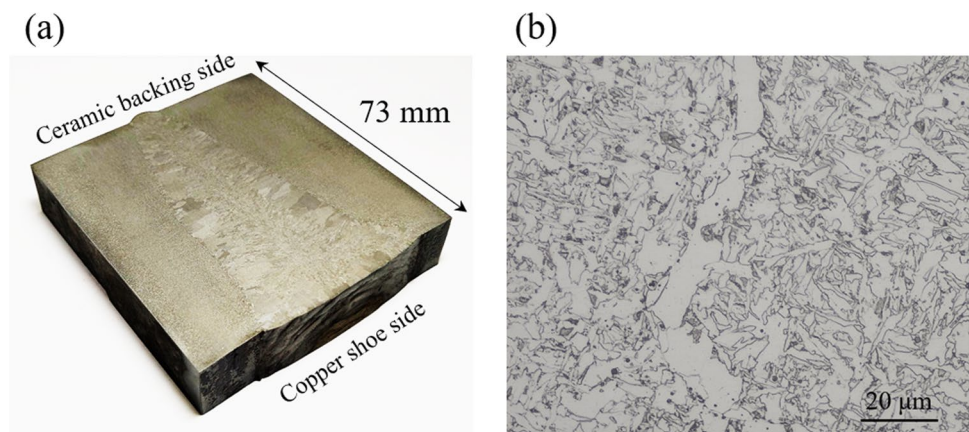


Fig. 2 SEM micrograph showing the AF plates grown from the inclusions

of Fig. 3, all the inclusions examined were almost entirely covered with the titanium-rich layer that was often noted to contain nitrogen to some extent.

Another example of a titanium-rich layer formed on the inclusion surface is shown in Fig. 4. Again, the inclusion is fully covered by titanium-rich layer, being a general feature of the present weld. One thing to note in the nitrogen image of Fig. 4 is that this layer contains much less nitrogen in comparison to that of the previous inclusion in Fig. 3. Instead, this inclusion has many titanium-rich particles that are high in nitrogen content. Of note are these particles being formed in two different morphologies at two different locations: plate-shape particles embedded in the silicate matrix and patch-type particles stuck on the inclusion surface. These two can be noted to be different in nitrogen content, patch-type being higher than the plate-type. Such difference in nitrogen content could be confirmed by EDS spot analyses performed at two locations of P and R, which

Fig. 1 EG weld investigated in this study: **a** three-dimensional view of specimen with the macrostructure revealed on the transverse cross section and **b** optical microstructure taken at the central region of weld metal. All specimens were etched with 2% Nital solution



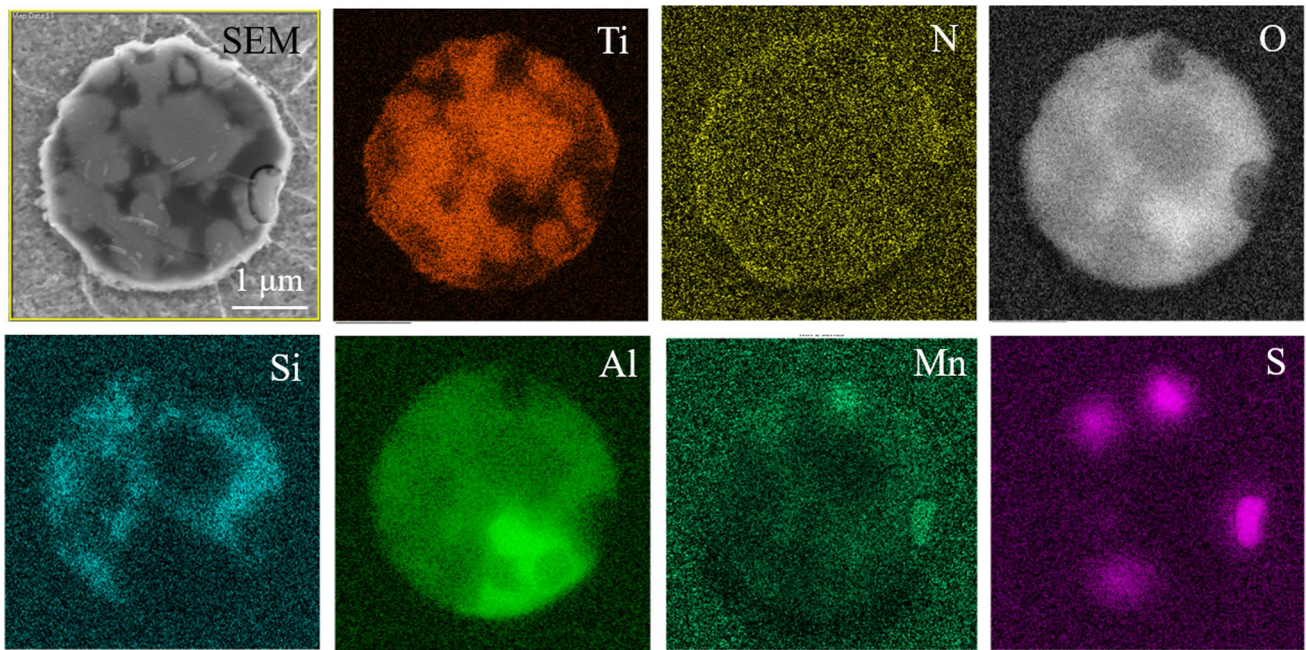


Fig. 3 SEM/EDS elemental mapping images taken from the cross-section of inclusion. Note the titanium-rich layer formed on the inclusion surface contains nitrogen

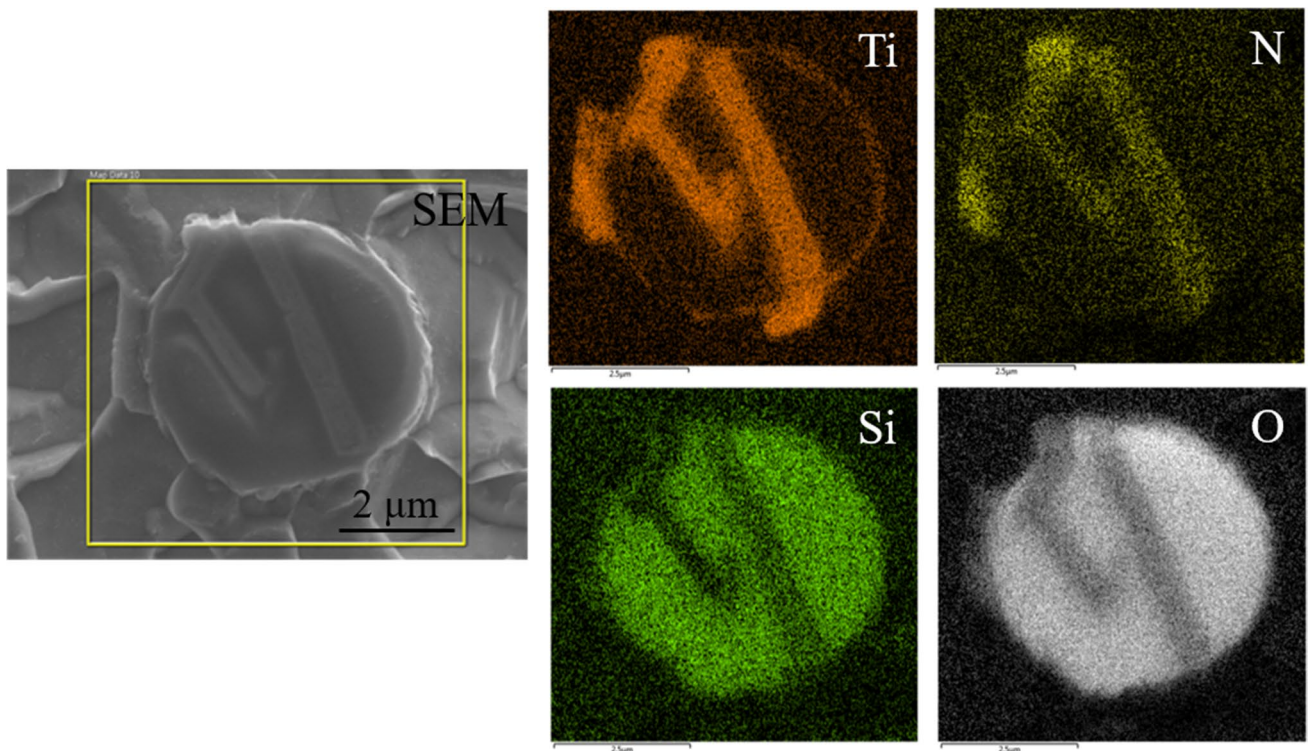


Fig. 4 SEM/EDS mapping images of titanium, silicon, nitrogen, and oxygen taken from the cross-section of inclusion. Titanium mapping image shows three different types of Ti-rich phase: plate, layer, and patch in shape

Fig. 5 Results of EDS spot analysis at locations of **a** R and **b** P

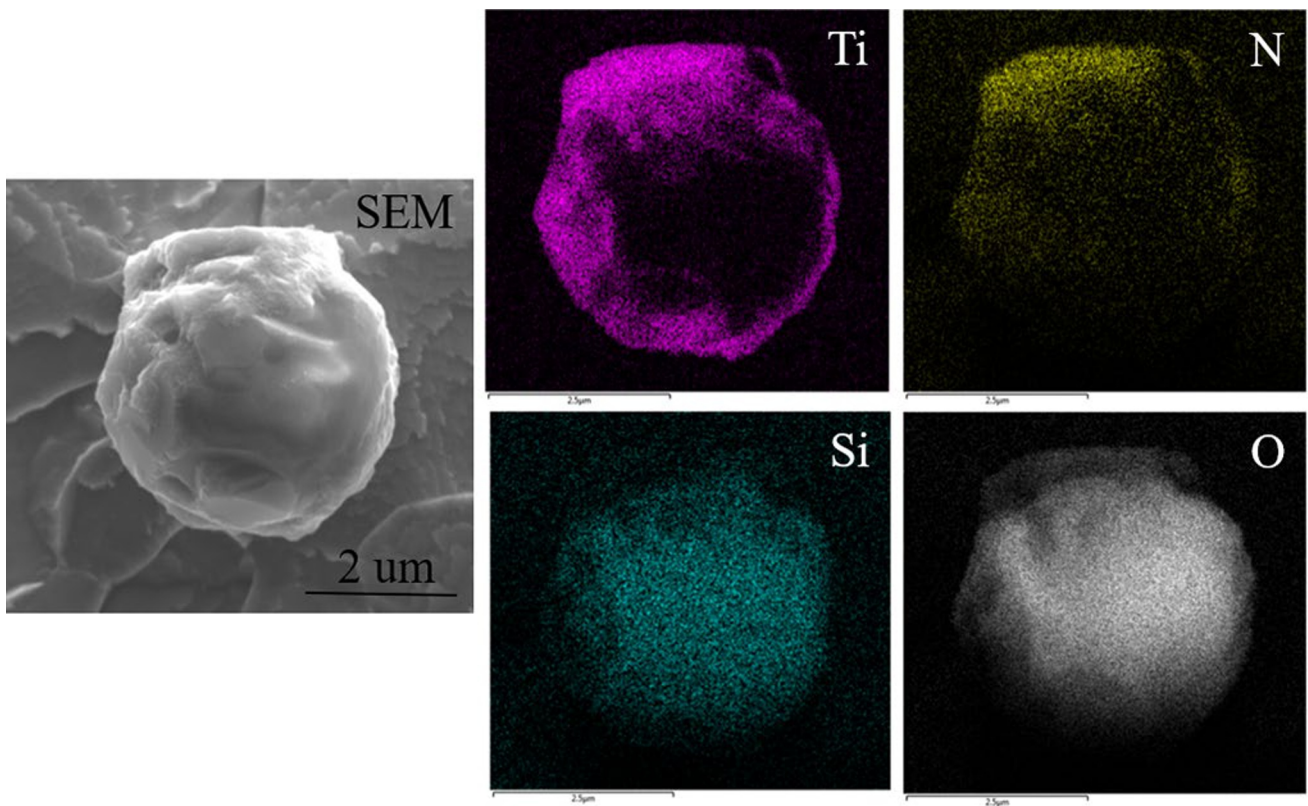
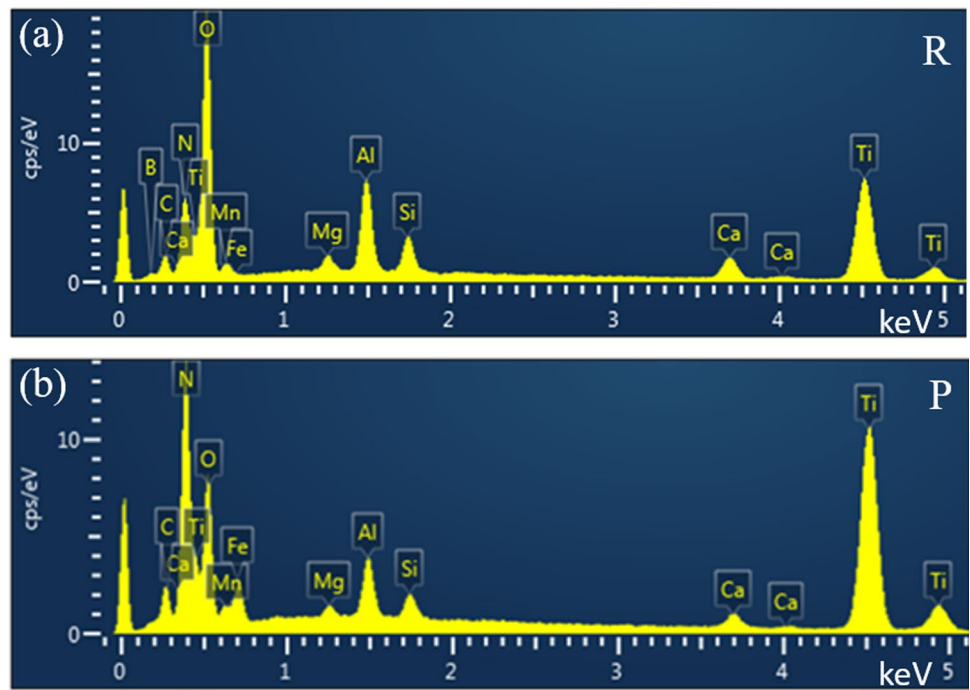


Fig. 6 SEM/EDS mapping images taken from the entire volume of inclusion exposed by deep etching technique

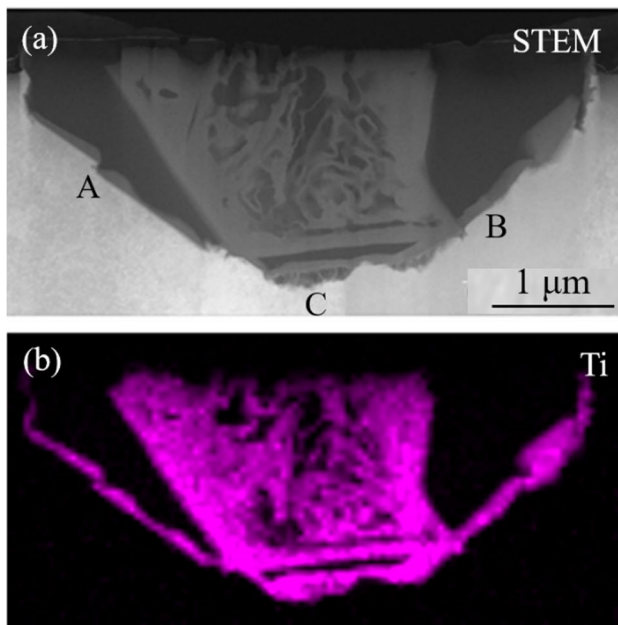


Fig. 7 ATEM results showing the images of **a** STEM and **b** titanium mapping by EDS

are representing patch-type and plate-type, respectively. As shown in Fig. 5, the nitrogen peak at point P is higher than the oxygen while that at point R is substantially lower than oxygen. It can be inferred from these EDS results that the plate particles formed in the matrix are a kind of titanium oxide alloyed with some nitrogen while the patch-type ones on the surface are predominant with TiN.

It was interesting to note that the plate shape of titanium oxides is quite different from that found previously in the low-nitrogen EG weld in that they were all globular in shape, suggesting that the shape of titanium oxide phase formed within the silicate matrix is determined by its nitrogen content which is largely controlled by the nitrogen content of the weld. Thus, it appears plausible to conclude that the titanium oxide changes its shape from globular to rectangular with increasing the nitrogen content of EG welds. The underlying mechanisms for this and the transition content of nitrogen were not clearly understood. Also noted for the patch-type phases were their size being much greater than that of EG(25t) weld previously examined. This enabled us to examine its nitrogen content even at a resolution level of EDS in SEM. As it appeared to be more like TiN, further examination has been performed on this phase.

Increasing the etching time allowed to expose the whole volume of inclusions on the etching surface, and Fig. 6 shows the SEM and EDS images taken from one of

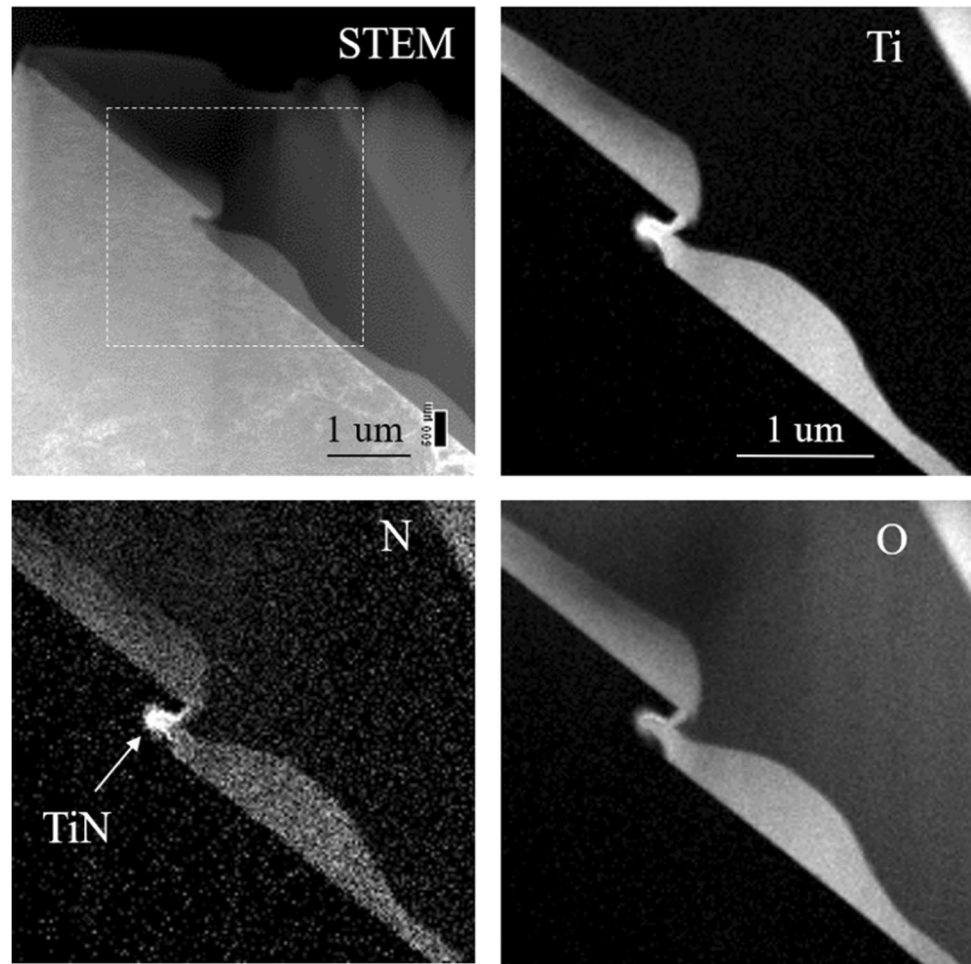
the inclusions partly covered by patch-type TiN particles. From this image, it can be noted that the patch-type TiN phase is not uniform in thickness and has a very rough surface, which is in contrast to the bulk surface partly exposed by the absence of TiN patches. EDS mapping results in Fig. 6 also demonstrate that this patch phase is not pure TiN but contains some aluminum and oxygen. This fact was reconfirmed in the ATEM analysis.

3.3 Inclusion analysis by ATEM/EDS/EELS

As observed in SEM examination (Fig. 4), the titanium-rich phases formed on the inclusion surface possess two different forms: layer-type or patch-type. To identify the chemical nature of each type, TEM study was performed using the specimens extracted by FIB system. The first inclusion examined was the one selected to characterize the layer-type titanium-rich phase which was shown in Fig. 3. Figure 7 shows its STEM and titanium mapping images, demonstrating the formation of continuous titanium-rich layer covering the whole inclusion surface. As this study concerns if TiN forms on the surface, an EELS examination was performed after thinning the specimen by ion milling. The EELS examination has a special advantage for this study as the absorption edges for oxygen, nitrogen, and titanium in EELS spectrum are better separated than those in an EDS spectrum, resulting in more precise and reliable analysis for these elements. For this inclusion, EELS analysis was conducted on three different areas marked as A, B, and C in Fig. 7a. Before EELS examination, these areas were observed at a high magnification and it was noted that the interfaces between layer and steel matrix in the regions of A and B were clean and straight while that in region C appeared to be wavy and rather rough.

Figure 8 shows the results obtained from region A in Fig. 7a: a high-magnification STEM image and EELS mapping results taken from the dotted area in the STEM image. The STEM image clearly shows that the titanium-rich layer forms and grows from the inner surface of inclusion. Such a growth pattern could result in a curved interface at the inclusion side and thus the layer thickness varies substantially. EELS mapping results also demonstrate that the titanium layer is very high in oxygen but contains a small amount of nitrogen. SAD analysis performed separately showed this phase has FCC structure with a lattice parameter of 0.42 nm. This can be attributed to TiO, TiN, TiC, or a combination of these phases, the lattice parameters of which are all in the range of accuracy permitted by SAD analysis. Combining this with EELS results, this layer could be determined to be TiO containing a small amount of nitrogen, which can be expressed

Fig. 8 STEM image of region A in Fig. 7a and the EELS mapping images of titanium (Ti), oxygen (O), and nitrogen (N) taken from the dotted box area in STEM image



in the form of $\text{Ti}(\text{O},\text{N})$. Recently, this type of TiO -rich layer has been reported to be found on the surface of inclusions of SAW weld metals and was also presented as $\text{Ti}(\text{O},\text{N})$ [36]. In Fig. 8, it is also worth noting the nitrogen-enriched, small and spherical particle present at the tip of the layer since this particle can represent a possible formation of TiN phase that has been expected in the present weld.

In contrast, as shown in the STEM image in Fig. 9, the titanium-rich layer observed in the region B was uniform in thickness of about 100 nm and most importantly, turned out to be composed of two sub-layers; the outer layer bordering the steel matrix is extremely thin, less than 10 nm. EELS mapping demonstrated that these two layers are far different in nitrogen content in that the outer layer is very high in nitrogen. The inner layer is predominantly titanium oxide containing a small amount of nitrogen, which is pretty much the same as that in Fig. 8. In fact, this layer was also determined to be TiO by the SAD analysis. SAD analysis also showed that the thin outer layer has the same crystal structure

as the inner layer, so this layer was suspected to be TiN from its high nitrogen content. To understand the relative content of oxygen and nitrogen in each layer, EELS line scanning was performed across the layer and its results are presented in Fig. 10. For the thick inner layer, the relative atomic concentration of titanium, oxygen, and nitrogen is approximately 5:4:1, suggesting this layer is a solid solution of TiO and TiN with a volume fraction of 4:1. In contrast, the outer layer is nearly absent from oxygen and thus can be identified to be pure TiN . The high-resolution lattice image taken from the interface between these two layers is shown in Fig. 11, demonstrating the epitaxial alignment of TiN with respect to TiO . The (111) lattice planes of TiO run into the (111) planes of TiN , demonstrating that the crystallographic orientations of TiO and TiN are identical. Therefore, it can be concluded that pure TiN phase indeed forms in this weld. Considering that TiN layer is present on the outer surface of TiO layer, it was inferred that TiO layer provides TiN with a substrate energetically favorable for its formation as TiO has nearly zero misfit with TiN .

Fig. 9 STEM image of region B in Fig. 7a and the EELS mapping images of titanium (Ti), oxygen (O), and nitrogen (N) taken from the dotted box area given in STEM image

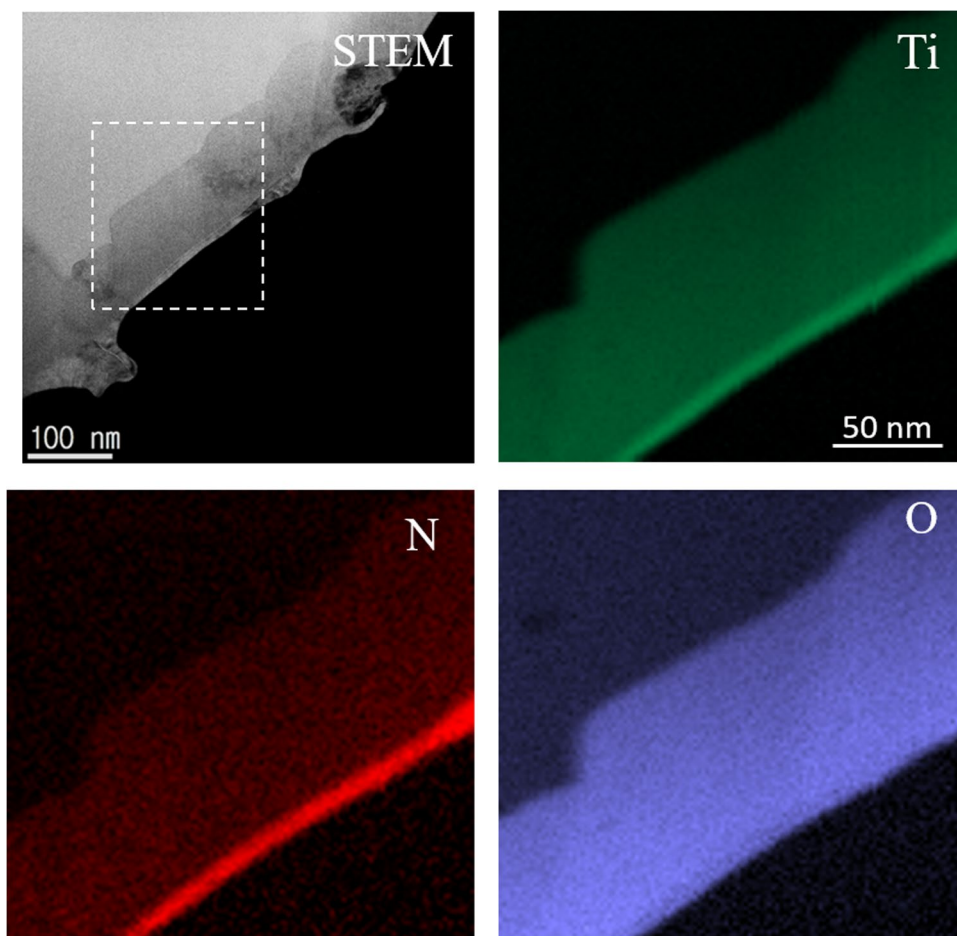
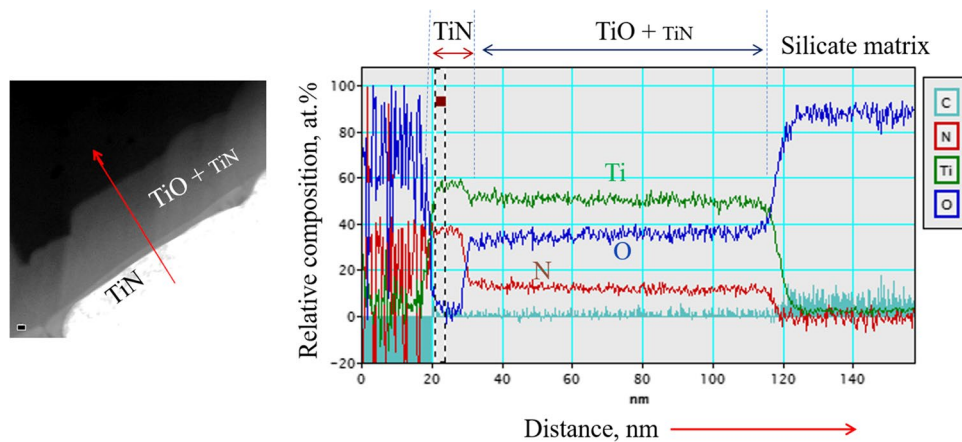


Fig. 10 Result of EELS line scanning across the titanium-rich layer showing the relative content of oxygen and nitrogen in each sub-layer



Lastly, the results of STEM and EELS analysis performed for the region C are presented in Fig. 12. These images clearly show that the titanium-rich phase formed here is different in that it is a kind of patch-type. This phase was confirmed to be formed on the outer surface of TiN/TiO layer and high in nitrogen content but surprisingly, was very complex in nature. At a glance, it

appears to be a mixture of TiN and some oxides containing manganese. In this context, it seemed to be of value to investigate this type of phase in more detail employing an inclusion having patches bigger in size, as like the one shown in Fig. 4. One of the inclusions selected from SEM observation for this purpose and examined in ATEM is presented in Fig. 13. From the STEM image, it

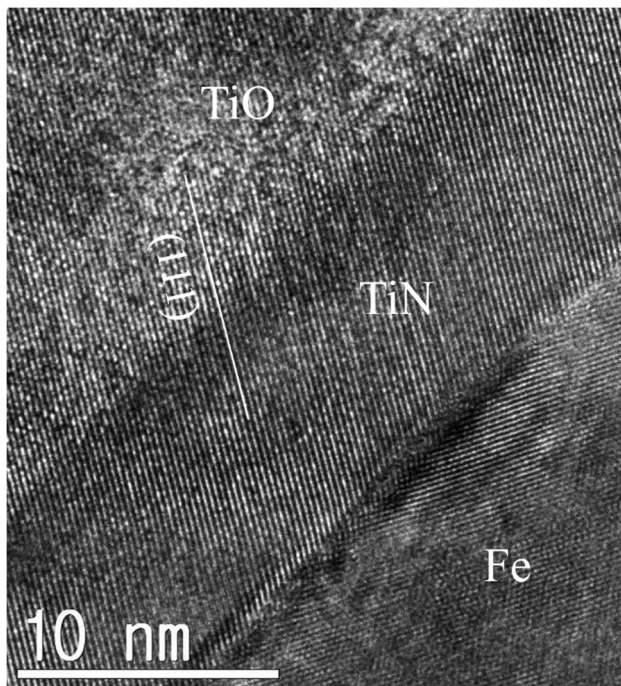


Fig. 11 High-resolution lattice image showing the (111) planes of TiO and TiN layers

can be seen that a half of this inclusion is fully covered with thick patches enriched with titanium and nitrogen. Its thickness was in a range of 100~200 nm. The STEM image also shows by different contrast that three ferrite grains (AF1, AF2, and AF3) were nucleated and grown from this inclusion and two of them were from the patch surfaces. In addition, these phases appeared to be a kind of lamellar mixture of two phases different in titanium content. Thus, to get a better understanding on the morphological feature and chemical inhomogeneity, further investigation was performed at high magnification for region “A” noted in the STEM image of Fig. 13.

The STEM image shown in Fig. 14 clearly demonstrates the formation of lamellar structure in the upper part of the patch: bright phase being rich in titanium and nitrogen, and the dark phase rich in aluminum, manganese, and oxygen. From these results, the bright and dark phase could be identified to be TiN and (Al,Mn)-oxide, respectively. Although the formation mechanism of lamellar mixture was not fully understood, it was for sure that this mixture formed at the last stage of inclusion formation as the patch phases were locating always on the outer surface of inclusion. The outer surface of inclusion

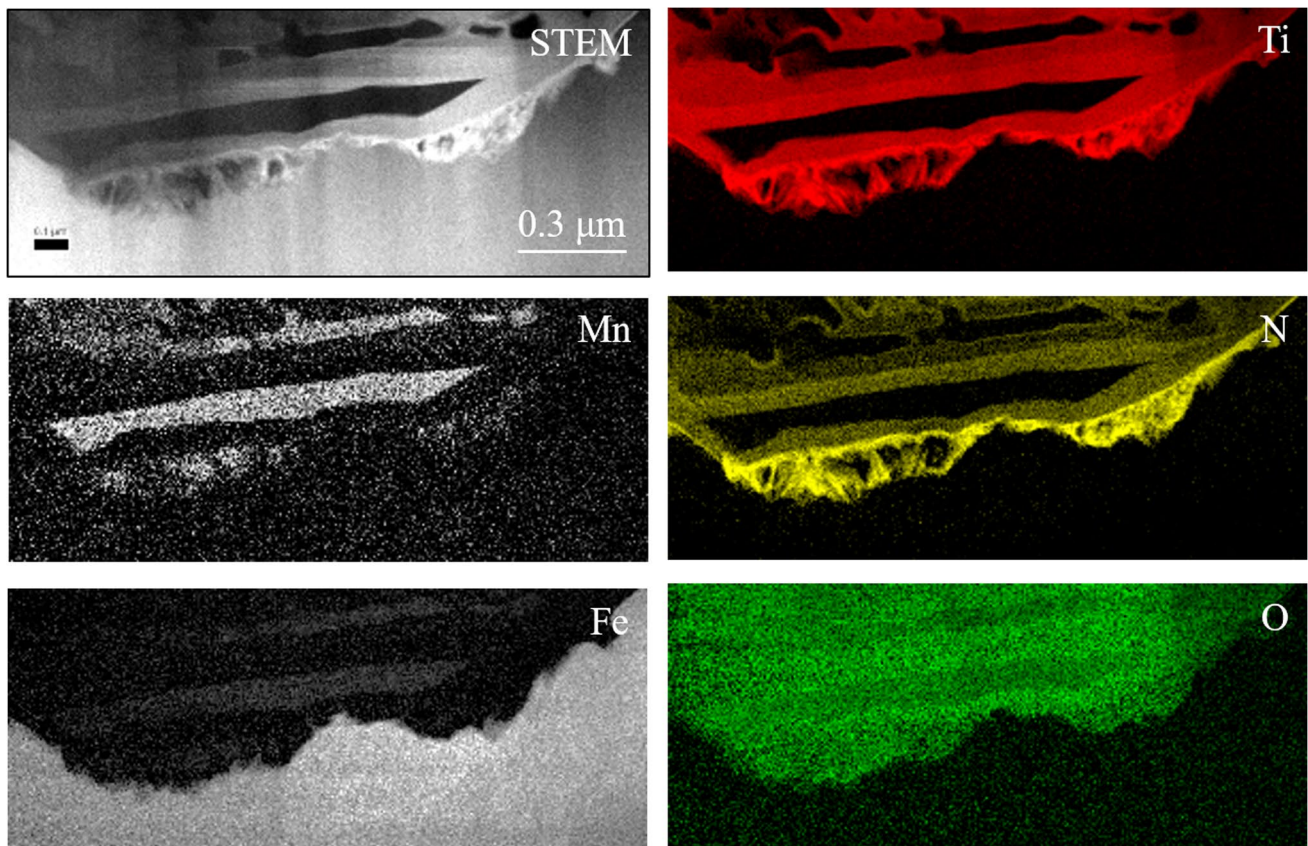


Fig. 12 STEM image of region C in Fig. 7a and the EELS mapping images of titanium (Ti), manganese (Mn), iron (Fe), nitrogen (N), and oxygen (O)

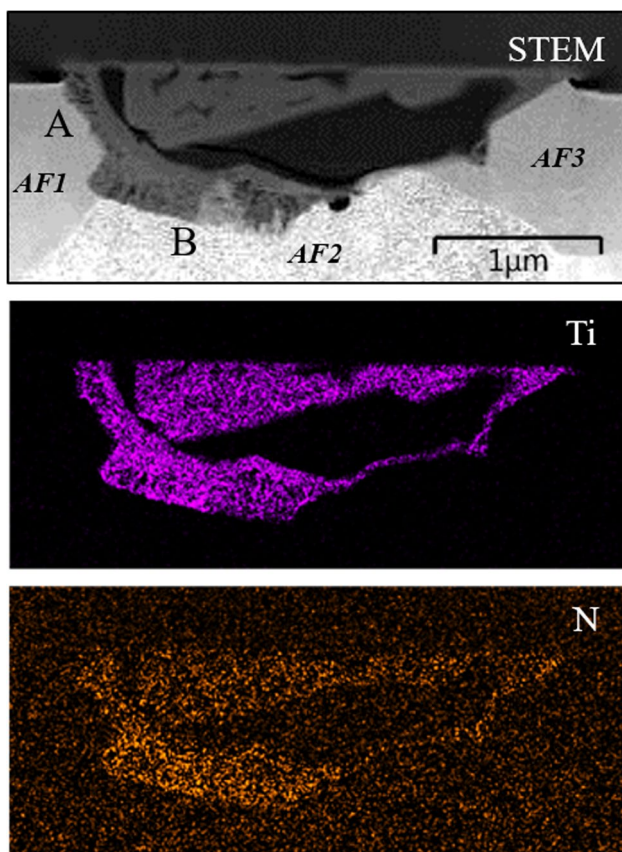


Fig. 13 ATEM results of the inclusion with thick patches at a low magnification: STEM image and the EDS mapping images of titanium (Ti) and nitrogen (N). In the STEM image, AF1, AF2, and AF3 are three ferrite grains nucleated from the inclusion

is composed of two sub-layers different in nitrogen and oxygen contents: one outside being TiN-dominant but that inside TiO-dominant.

SAD patterns taken from region A are shown in Fig. 15, demonstrating that the titanium-rich phases in the patch are indeed TiN having the same orientation with TiN/TiO layers and showing Baker-Nutting (B-N) orientation relation with ferrite matrix but with a slight misalignment between (200) planes. This result indicates the TiN phase in this patch is effective for the ferrite formation. Effectiveness of patch-type TiN was also supported by the SEM observations of ferrite grains grown from the patches, as shown in Fig. 16. Nonetheless, the relative potency of TiN with respect to TiO could not be assessed.

4 Conclusion

An investigation has been carried out of the chemical and crystal nature of titanium-rich layer formed on the surface of inclusions in a high-nitrogen tandem EG weld metal to establish a better understanding of the morphological characteristics of TiN phase. The following conclusions have been drawn:

- (1) Inclusions examined in the present EG weld were fully covered with the titanium-rich layer, and this layer was partly coated with another type of titanium-rich phase called patch-type.

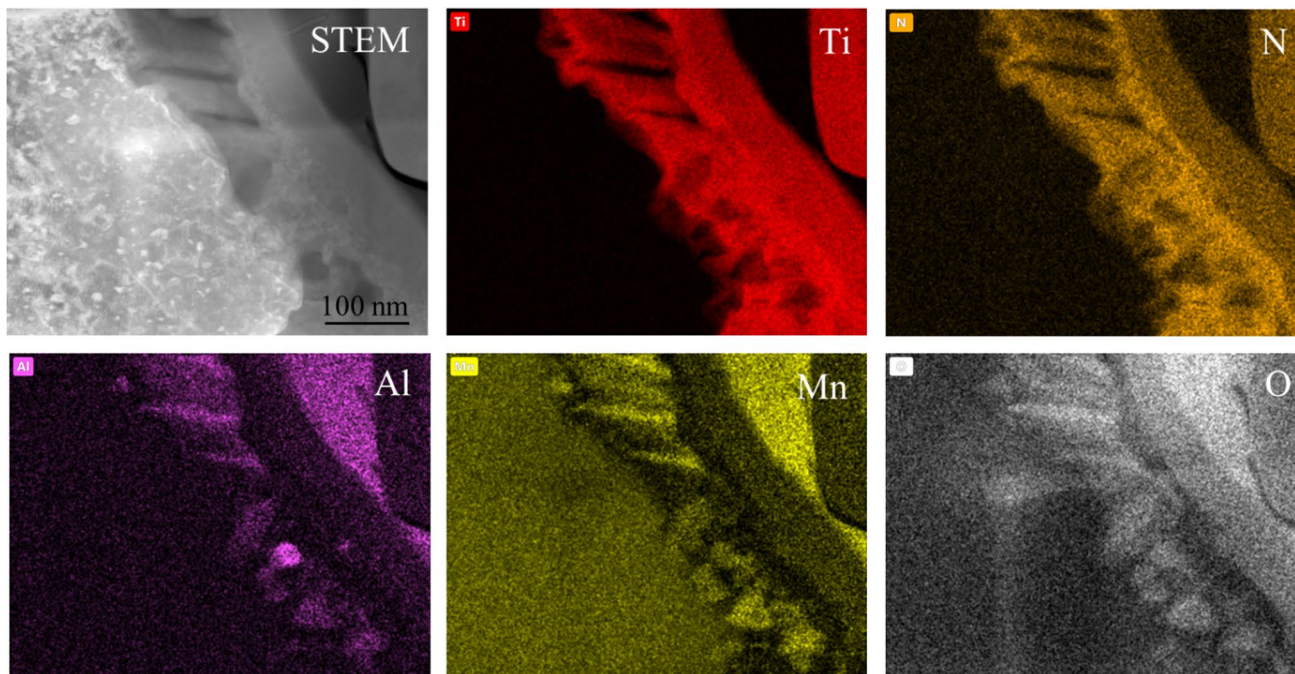


Fig. 14 ATEM results obtained from the region A in Fig. 13: STEM image and the EDS mapping images of titanium (Ti), nitrogen (N), aluminum (Al), manganese (Mn), and oxygen (O)

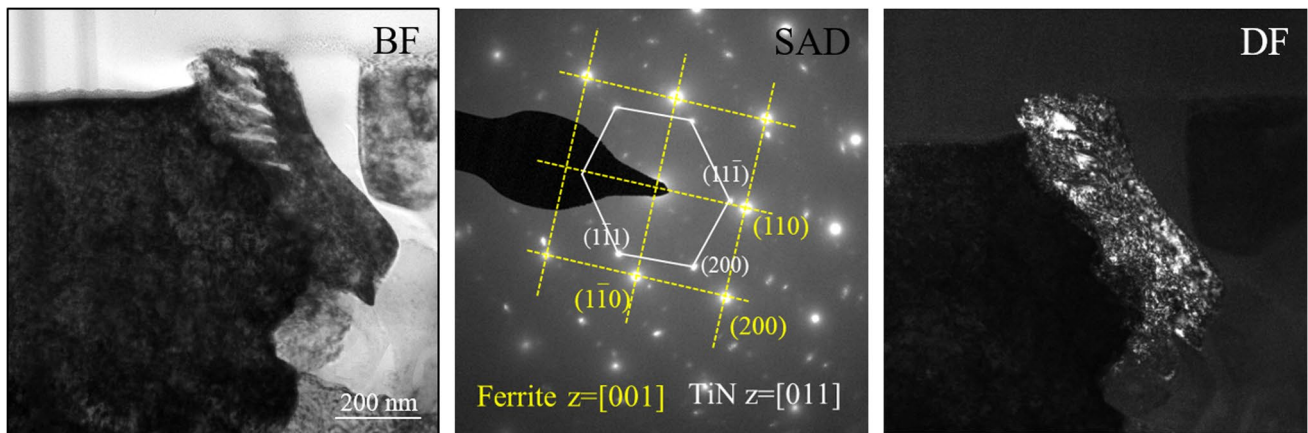
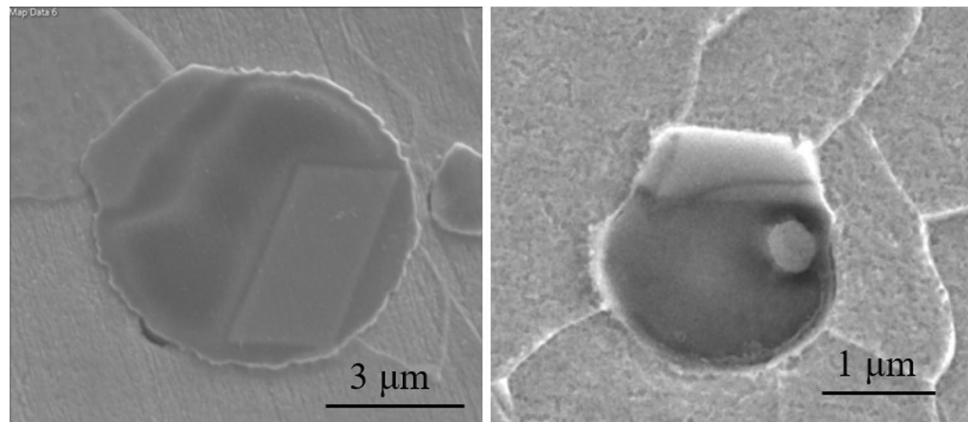


Fig. 15 Results of SAD analysis performed for region A: bright field (BF) image, SAD pattern showing B-N orientation relation and dark field (DF) image taken from (111) spot of TiN

Fig. 16 Inclusions partly covered with patches acting as nucleation sites for ferrite grains



- (2) Titanium-rich layer was either a single layer of TiO containing some nitrogen or a double layer of TiO and TiN, TiN layer being formed on the outer surface of TiO. The crystal orientations of these two layers were the same.
- (3) Patch-type has a mixture of TiN and (Al,Mn)-oxide, being formed in a lamellar structure and grown from the outer surface of TiN layer. Thus the orientation of TiN phase in the patch was the same as that of TiN/TiO layer.
- (4) Patch-type phases were confirmed to act as the nucleation sites of ferrite grains but their relative potency of ferrite nucleation to TiO layer could not be determined.

Open Access This article is licensed under a Creative Commons Attribution 4.0 International License, which permits use, sharing, adaptation, distribution and reproduction in any medium or format, as long as you give appropriate credit to the original author(s) and the source, provide a link to the Creative Commons licence, and indicate if changes were made. The images or other third party material in this article are included in the article's Creative Commons licence, unless indicated otherwise in a credit line to the material. If material is not included in the article's Creative Commons licence and your intended use is not permitted by statutory regulation or exceeds the permitted use, you will need to obtain permission directly from the copyright holder. To view a copy of this licence, visit <http://creativecommons.org/licenses/by/4.0/>.

Funding This study was supported by the Fundamental Research Program of the Korea Institute of Material Science (KIMS) (grant no. PNK 8210).

Declarations

Conflict of interest The authors declare no competing interests.

References

1. Sarma DS, Karasev AV, Jonsson PG (2009) On the role of non-metallic inclusions in the nucleation of acicular ferrite in steels. *ISIJ Int* 49(7):1063–1074
2. Evans GM (1992) The effect of titanium in SMA C-Mn steel multipass deposits. *Weld J* 71(12):447s–454s

3. Evans GM (1993) The effect of titanium in manganese-containing SMA weld deposits. *Weld J* 72(3):123s–133s
4. Evans GM (1995) Microstructure and properties of ferritic steel welds containing Al and Ti. *Weld J* 74(8):249s–261s
5. Evans GM (1996) Microstructure and properties of ferritic steel welds containing Ti and B. *Weld J* 75(8):251s–260s
6. Johnson MQ, Evans GM, Edwards GR (1995) The influence of titanium additions and interpass temperature on the microstructures and mechanical properties of high strength SMA weld metals. *ISIJ Int* 36(10):1222–1231
7. Horii Y, Ichikawa K, Ohkita S, Funaki S, Yurioka N (1995) Chemical composition and crystal structure of oxide inclusions promoting acicular ferrite transformation in low alloy submerged arc weld metal. *Quarterly J JWS* 13(4):500–507
8. Yamata T, Terasaki H, Komizo Y (2009) Relation between inclusion surface and acicular ferrite in low carbon low alloy steel welds. *ISIJ Int* 49(7):1059–1062
9. Takada A, Terasaki H, Komizo Y (2013) Effect of aluminum content on acicular ferrite formation in low carbon steel weld metals. *Sci Tech Weld Join* 18(2):91–97
10. Fujiyama N, Shigasato G (2011) Effects of Mn and Al on acicular ferrite formation in SAW weld metal. *ISIJ Int* 61(5):1614–1622
11. Blais C, L'Esperance G, Evans GM (1999) Characterization of inclusions found in C-Mn steel welds containing titanium. *Sci Tech Weld Join* 4(3):143–150
12. Nako H, Hatano H, Okazaki Y, Yamashita K, Otsu M (2014) Crystal orientation relationship between acicular ferrite, oxide, and the austenite matrix. *ISIJ Int* 54(7):1690–1696
13. Seo K, Kim K, Kim HJ, Ryoo H, Evans GM, Lee C (2020) Microstructural and inclusion characteristics of C-Mn steel welds at a minimal level of titanium. *Met Mater Int* 26(8):1226–1234. <https://doi.org/10.1007/s12540-019-00390-4>
14. Kang Y, Jeong S, Kang J-H, Lee C (2016) Factors affecting the inclusion potency for acicular ferrite nucleation in high-strength steel welds. *Metal Mater Tran A* 47A(6):2842–2854. <https://doi.org/10.1007/s11661-016-3456-0>
15. Kang Y, Lee C (2016) Nucleation behavior of acicular ferrite in 1 GPa class high strength steel weld metal. *J Weld Join* 37(1):21–26 (in Korean)
16. Seo JS, Kim HJ, Lee C (2013) Effect of Ti addition on weld microstructure and inclusion characteristics of bainitic GMA welds. *ISIJ Int* 53(5):880–886. <https://doi.org/10.2355/isijinternational.53.880>
17. Seo K, Kim Y, Evan GM, Kim HJ, Lee C (2015) Formation of Mn-depleted zone in Ti-containing weld metals. *Weld World* 59:373–380. <https://doi.org/10.1007/s40194-014-0207-y>
18. St-Laurent S, L'Esperance G (1992) Effects of chemistry, density and size distribution of inclusions on the nucleation of acicular ferrite of C-Mn steel shielded-metal-arc-welding weldments. *Mater Sci Eng A* 149:203–216
19. Kluken AO, Grong Ø (1989) Mechanisms of inclusion formation in Al-Ti-Si-Mn deoxidized steel weld metals. *Met Trans A* 20A(8):1335–1349
20. Tomita Y, Saito N, Tsuzuki T, Tokunaga Y, Okamoto K (1994) Improvement in HAZ toughness of steel by TiN-MnS addition. *ISIJ Int* 24(10):829–835
21. Morikage Y, Oi K, Kawabata F, Amano K (1998) Effect of TiN size on ferrite nucleation on TiN in low-C steel. *Tetsu-to-Hagane* 84(7):510–515 (in Japanese)
22. Jin H-H, Shim J-H, Cho YW, Lee H-C (2003) Formation of intragranular acicular ferrite grains in a Ti-containing low carbon steel. *ISIJ Int* 43(7):1111–1113
23. Lee C, Nambu S, Inoue J, Koseki T (2011) Ferrite formation behavior from B1 compounds in steels. *ISIJ Int* 51(12):2036–2041
24. Mu W, Jönsson PG, Shibata H, Nakajima K (2016) Inclusion and microstructure characteristics in steels with TiN additions. *Steel Research Int* 87(3):339–348
25. Gregg JM, Bhadeshia HKDH (1994) Titanium-rich mineral phases and the nucleation of bainite. *Metal Mater Trans A* 25(8):1603–1611
26. Gregg JM, Bhadeshia HKDH (1997) Solid-state nucleation of acicular ferrite on minerals added to molten steel. *Acta Mater* 45(2):739–748
27. Shim JH, Oh YH, Sun JY, Cho YW, Shim JD, Byun JS, Lee DN (2001) Ferrite nucleation potency of non-metallic inclusions in medium carbon steels. *Acta Mater* 49:2115–2122. www.elsevier.com/locate/actamat
28. Shi M, Zhang P, Zhu F (2014) Toughness and microstructure of coarse grain heat affected zone with high heat input welding in Zr-bearing low carbon steel. *ISIJ Int* 54(1):188–192. <https://doi.org/10.2355/isijinternational.54.188>
29. Ito Y, Nakanishi M (1975) Study on Charpy impact properties of welds (Report 2). *Journal of JWS* 44(10):815–821
30. Lau TW, Sadowski MM, North TH, Weatherly GC (1988) Effect of nitrogen on properties of submerged arc weld metal. *Mater Sci Tech* 4(1):52–61
31. Grong Ø, Kluken AO, Nylund HK, Dons AL, Hjelen J (1995) Catalyst effects in heterogeneous nucleation of acicular ferrite. *Met Trans A* 26A(3):525–534
32. Seo K, Ryoo H, Kim HJ, Yoon JG, Lee C (2022) Nature of non-metallic inclusions in electrogas weld metal. *Weld World* 66(2):379–390. <https://doi.org/10.1007/s40194-021-01246-5>
33. Choi W, Matsuura H, Tsukihashi F (2013) Effect of nitrogen on the formation and evolution of non-metallic inclusions in Fe-Al-Ti-N alloys. *ISIJ Int* 53(11):2007–2012
34. Seo K, Ryoo H, Kim HJ, Yoon JG, Lee C (2020) Characterization of the local brittle layer formed in electro-gas weld metals. *Weld World* 65(3):513–524. <https://doi.org/10.1007/s40194-020-01032-9>
35. Kojima A, Kasuya T, Tsuruta T, Minami K (2007) Study on application of electrogas arc welding to SM570 steel in bridge fabrication. *Trans Japanese Society of Civil Eng A* 63(1):1–13 (in Japanese)
36. Fujiyama N, Shigesato G (2021) Effects of Mn and Al on acicular ferrite formation in SAW weld metal. *ISIJ Int* 61(5):1614–1622. <https://doi.org/10.2355/isijinternational.ISIJINT-2020-407>

Publisher's note Springer Nature remains neutral with regard to jurisdictional claims in published maps and institutional affiliations.